

# Lanthanoid Single-Ion Magnets Based on Polyoxometalates with a 5-fold Symmetry: The Series $[\text{LnP}_5\text{W}_{30}\text{O}_{110}]^{12-}$ ( $\text{Ln}^{3+} = \text{Tb}, \text{Dy}, \text{Ho}, \text{Er}, \text{Tm}, \text{and Yb}$ )

S. Cardona-Serra,<sup>†</sup> J. M. Clemente-Juan,<sup>†</sup> E. Coronado,<sup>†,\*</sup> A. Gaita-Ariño,<sup>†</sup> A. Camón,<sup>‡</sup> M. Evangelisti,<sup>‡,§</sup> F. Luis,<sup>‡,§,\*</sup> M. J. Martínez-Pérez,<sup>‡,§</sup> and J. Sesé<sup>§,⊥</sup>

<sup>†</sup>Instituto de Ciencia Molecular (ICMol), Universidad de Valencia, Catedrático José Beltrán Martínez No. 2, 46980 Paterna, Spain

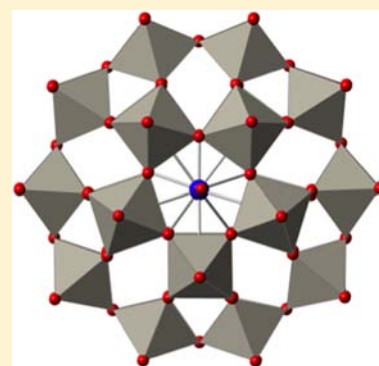
<sup>‡</sup>Instituto de Ciencia de Materiales de Aragón (ICMA), CSIC-Universidad de Zaragoza, Plaza San Francisco s/n, 50009 Zaragoza, Spain

<sup>§</sup>Departamento de Física de la Materia Condensada, Universidad de Zaragoza, Plaza San Francisco s/n, 50009 Zaragoza, Spain

<sup>⊥</sup>Instituto de Nanociencia de Aragón (INA), Universidad de Zaragoza, Edificio I+D, Campus Río Ebro, 50018 Zaragoza, Spain

## Supporting Information

**ABSTRACT:** A robust, stable and processable family of mononuclear lanthanoid complexes based on polyoxometalates (POMs) that exhibit single-molecule magnetic behavior is described here. Preyssler polyanions of general formula  $[\text{LnP}_5\text{W}_{30}\text{O}_{110}]^{12-}$  ( $\text{Ln}^{3+} = \text{Tb}, \text{Dy}, \text{Ho}, \text{Er}, \text{Tm}, \text{and Yb}$ ) have been characterized with static and dynamic magnetic measurements and heat capacity experiments. For the Dy and Ho derivatives, slow relaxation of the magnetization has been found. A simple interpretation of these properties is achieved by using crystal field theory.



## INTRODUCTION

The relevance of polyoxometalates (POMs) in molecular magnetism is based on the ability of these metal-oxide clusters to act as chelating ligands incorporating a large number of magnetic centers at specific sites of their molecular structures.<sup>1</sup> Magnetic POMs can be divided into three broad families. A first class consists of POMs encapsulating a number of 3d-transition metal ions, which can be connected through oxo bridges forming magnetic clusters of variable nuclearities and high symmetries, often enabling exchange interactions between the magnetic centers. A second family is formed by POMs encapsulating one or more lanthanoid ions in order to give rise to a lanthanoid complex in which the 4f-magnetic ions are submitted to the crystal field created by the POM ligands. Finally, a third family incorporates a mixed-valence POM framework hosting a number of electrons that are usually hopping over all the framework structure. The result is a mixed-valence magnetic POM in which the localized magnetic moments coming from the encapsulated 3d or 4f metal ions are coexisting or even interacting with the delocalized electrons coming from the POM framework.<sup>2,3</sup>

In all these cases, the rigidity and large size of the generally nonmagnetic POM framework lead to magnetic systems possessing highly symmetric topologies and coordination sites, while keeping an effective magnetic isolation between

them and a remarkable stability in solution as well as in the solid state.<sup>4</sup> Owing to all these electronic, structural, and chemical features, the studies of magnetic POMs give precise and unique answers to the questions of magnetic interactions.<sup>1,5-7</sup>

Taking advantage of all this previous knowledge, we are now in position of using these polyanions as platforms for designing magnetic molecules exhibiting useful properties such as magnetic bistability or switching, which can open new perspectives in molecular spintronics and quantum computing.<sup>8-10</sup> A key result in this context was the discovery in 2008 of the first examples of mononuclear lanthanoid POMs behaving as single-molecule magnets (SMMs).<sup>11</sup> Thus, it was demonstrated that the sodium salt of the polyanion  $[\text{Er}(\text{W}_5\text{O}_{18})_2]^{9-}$  exhibits a slow relaxation of the magnetization at low temperatures, which agrees with the presence of an energy barrier for the reversal of the magnetization very close to that observed for the archetypical  $\text{Mn}_{12}$  cluster ( $U_{\text{eff}}/k_B \approx 60$  K), and a very rich physics at very low temperature connected with quantum tunneling effects.<sup>12</sup> This kind of POM possesses an octacoordinated coordination site close to the antiprismatic  $D_{4d}$  symmetry. It represents the second example of a mononuclear

Received: June 1, 2012

Published: August 15, 2012

lanthanoid complex behaving as a SMM. The first example was discovered by Ishikawa et al. in 2003 in the Tb derivative of the bis-phthalocyaninato complexes formulated as  $[\text{LnPc}_2]^-$ , also possessing a  $D_{4d}$  symmetry.<sup>13</sup> In this class of mononuclear nanomagnets, also known as single-ion magnets (SIMs), the magnetic anisotropy required for observing this barrier arises from the splitting of the  $J$  ground state of the  $\text{Ln}^{\text{III}}$  when it is submitted to a crystal field (CF). For certain CF symmetries, such splitting can stabilize sublevels with a large  $|M_J|$  value, thus achieving an easy axis of the magnetization.<sup>14</sup> In these two cases, the different distortion of the antiprismatic site (axially compressed for POMs and axially elongated for the  $[\text{LnPc}_2]^-$  complexes) leads to a different splitting of the  $\pm M_J$  levels. Thus, these coordination sites stabilize the higher  $M_J$  values in the Er derivative encapsulated by POMs or in the Tb derivative encapsulated by phtalocyanines. That explains why these two mononuclear complexes behave as SMMs. In these systems, the slow relaxation of the magnetization is ensured by the highly symmetrical coordination symmetry around the lanthanoid, such as the pseudoaxial  $D_{4d}$  symmetry, which favors the purity of the ground doublet. It seems obvious that many other lanthanoid complexes should satisfy these structural and electronic requirements. Still, most of the known examples of SIMs reported so far are restricted to the antiprismatic  $D_{4d}$  symmetry.

Other coordination geometries different from the  $D_{4d}$  need now to be explored. In fact, other axial symmetries around the lanthanide, such as  $D_{2d}$ ,<sup>15a</sup>  $D_{3h}$ ,<sup>15b</sup> and  $C_\infty$ ,<sup>15c</sup> have also shown to exhibit a SMM behavior. In the present paper, we will extend this study to other geometries taking advantage of the unique ability of POMs to act as rigid ligands offering a powerful tool for the design of metal complexes with tailored symmetries. We here focus on the well-known  $[\text{LnW}_{30}\text{O}_{110}]^{12-}$  family of complexes in which its very unusual  $C_5$  axial symmetry allows us to study both experimentally and theoretically the possibilities of preparing new SIMs having 5-fold symmetry.

## EXPERIMENTAL SECTION

**Synthesis.** All reactants and solvents were of commercially available grade and used without any previous purification.  $\text{LnCl}_3 \cdot 6\text{H}_2\text{O}$  are highly hygroscopic and should be stored in desiccators. The mixed potassium/sodium Preyssler salt, where a sodium ion is encapsulated, was prepared according to a well-known procedure<sup>16</sup> and identified by FT-IR techniques.

$\text{K}_{12}\text{LnP}_3\text{W}_{30}\text{O}_{110} \cdot n\text{H}_2\text{O}$  ( $\text{Ln}^{3+} = \text{Tb}, \text{Dy}, \text{Ho}, \text{Er}, \text{Tm}, \text{and Yb}$ ) was prepared following the previously described method.<sup>16</sup>

In a typical experiment,  $\text{K}_{12.5}\text{Na}_{1.5}[\text{NaP}_3\text{W}_{30}\text{O}_{110}] \cdot 15\text{H}_2\text{O}$  (1 g, 0.12 mmol) was dissolved in 12 mL of water, and the solution was heated to 60–70 °C. To this solution, 2 equiv of the lanthanoid ion, as the chloride salt dissolved in water, was added dropwise (3 mL). The mixture was placed in a Parr model 4746 or model 4748 sample preparation bomb and heated to 160 °C overnight. After the solution had cooled to room temperature, the product was isolated by the addition of 4 g of solid KCl. The product was identified by FT-IR: 1159(s), 1064(s), 1020(m), 939(s), 914(s), 777(s), 568(w), 539(m), 468(w).

**Physical Measurements.** IR spectra were recorded on a FT-IR Nicolet 5700 spectrometer in the 4000–400  $\text{cm}^{-1}$  range using powdered sample in KBr pellets. Magnetic susceptibility,  $\chi_m$ , data were measured between 2 and 300 K with a commercial magnetometer equipped with a SQUID sensor and a commercial physical properties measurement system (PPMS). The diamagnetic contributions to the susceptibility were corrected using Pascal's constant tables. Direct current (dc) data were collected with an applied field of 1000 Oe. Alternate current (ac) were collected in the range 2–12 K with an

applied alternating field of 3.95 Oe at different frequencies in the range 1–10000 Hz. The magnetic characterization was extended to very low temperatures with a combination of noncommercial experimental set-ups. Magnetization hysteresis loops were measured between 350 mK and 7 K using a homemade micro-Hall magnetometer working in a  $^3\text{He}$  refrigerator. The sample, mixed with Apiezon N grease to ensure its proper thermalization at these very low temperatures, was deposited directly on the edge of one of the two Hall crosses. The ac susceptibility of a powdered  $\text{DyW}_{30}$  sample was measured from 333 Hz to 13 kHz using a home-built mutual inductance susceptometer thermally anchored to the mixing chamber of a  $^3\text{He}$ – $^4\text{He}$  dilution refrigerator, which gives access to temperatures ranging from 0.09 to 3.5 K. The ac susceptibility of a  $\text{HoW}_{30}$  single crystal was measured, from 0.03 Hz to 200 kHz, using an integrated microSQUID susceptometer, recently developed by some of us,<sup>17</sup> which works in the temperature region from 13 mK to 3 K. Inelastic neutron scattering experiments were performed on the IN4 instrument of the Institut Laue-Langevin at wavelengths 1.1, 2.2, and 3.6 Å. Finally, specific heat data were also measured between 350 mK and 20 K on compact pellet samples using a commercial PPMS.

## RESULTS AND DISCUSSION

Here we report the magnetic study of a series of mononuclear lanthanoid-based complexes formulated as  $\text{K}_{12}\text{LnP}_3\text{W}_{30}\text{O}_{110} \cdot n\text{H}_2\text{O}$  ( $\text{Ln}^{3+} = \text{Tb}, \text{Dy}, \text{Ho}, \text{Er}, \text{Tm}, \text{and Yb}$ ), which are usually called “Preyssler anions” (see Figure 1a). In these complex systems the structural details depend on the experimental data available. We base our description of the structure on single-crystal X-ray results.<sup>18</sup>

In this POM structure, the lanthanoid cation can occupy two equivalent coordination sites, which show a very unusual 5-fold geometry formed by five phosphate oxygens ( $d_{\text{Ln}-\text{Op}} \approx 2.7 \text{ \AA}$ ) and five bridging oxygens between two tungsten atoms ( $d_{\text{Ln}-\text{Ow}}$

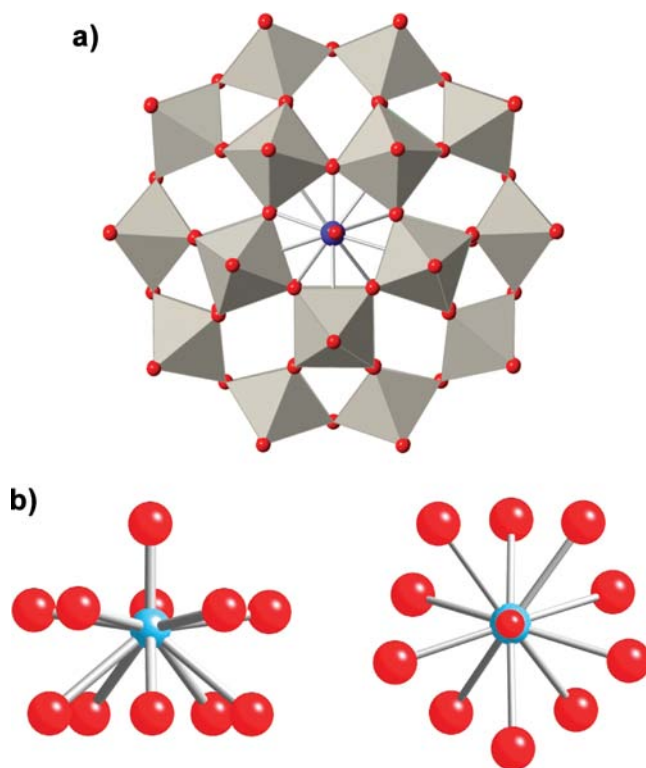


**Figure 1.** (a) Complete structure of the  $[\text{LnP}_3\text{W}_{30}\text{O}_{110}]^{12-}$  anion. (b) Scheme showing the coordination of the lanthanoid ion in a 5-fold environment.

$\approx 2.9 \text{ \AA}$ ). The result is a pentagonal antiprism coordination site (Figure 1b). The lanthanoid cation is not placed at the center of this antiprism but closer to the plane formed by the phosphate oxygens. A water molecule placed in an axial position close to the other coordination site completes the coordination sphere ( $d_{\text{Ln-O}} \approx 2.2 \text{ \AA}$ ). The coordination number of the lanthanoid cation is 11 (monocapped pentagonal antiprism, shown in Figure 1b). Based on these structural considerations, we assign an ideal  $C_5$  symmetry to the coordination of the lanthanoid ion in the whole series of  $[\text{LnP}_5\text{W}_{30}\text{O}_{110}]^{12-}$  POMs (in short  $\text{LnW}_{30}$ ). These anionic molecules are surrounded by potassium cations for charge balance. Given the size of the POM ligands that are encapsulating the lanthanoid, an extremely good isolation of the anisotropic  $\text{Ln}^{3+}$  ions in the solid state is observed (shortest  $\text{Ln-Ln}$  distance of  $13.2 \text{ \AA}$ ).

It is important to note that, despite the differences of the cited X-ray description with indirect techniques like spectroscopic lifetime measurements or EXAFS studies,<sup>25</sup> our geometrical reasoning is robust and does not change with fine details. In particular, and as discussed below, the 5-fold symmetry, which has not been put in doubt by any technique, is what produces  $A_6^5$  as only extradiagonal parameter. The diagonal terms  $A_2^0$ ,  $A_4^0$ , and  $A_6^0$  can similarly be interpreted in terms of polar angles and independently of small variations in the metal–ligand distance.

**Determination of Crystal Field Parameters.** Direct current magnetic measurements have been used to determine the CF parameters and the resulting splitting of the ground electronic state of the lanthanoid ions caused by the crystal field. One has to note that the substitution proportion  $x$  of sodium by lanthanoid cations in the structure is often not complete, with usual values in the range  $0.85 < x < 0.95$ . As already shown by Creaser et al.,<sup>19</sup> this effect is to be expected specially for  $\text{Tm}^{3+}$  and  $\text{Yb}^{3+}$ , with  $0.4 < x < 0.6$ . We account for this effect by a scaling factor of the whole  $\chi_m T$  curve, which, as shown in Table 1, produces a good agreement between the

**Table 1. Total Angular Momentum of the Lanthanoid Cations, as Given by Hund's Rules, and  $\chi_m T$  Values for  $\text{LnW}_{30}$  Family**

lanthanoid ion	$J$	$\chi_m T$ of the free ion (emu·K/mol)	$\chi_m T$ of the $\text{LnPOM}$ complex (emu·K/mol)
$\text{Tb}^{3+}$	6	11.81	11.48
$\text{Dy}^{3+}$	15/2	14.17	14.41
$\text{Ho}^{3+}$	8	14.06	14.386
$\text{Er}^{3+}$	15/2	11.475	11.37
$\text{Tm}^{3+}$	6	7.15	7.22
$\text{Yb}^{3+}$	7/2	2.57	2.51

room temperature  $\chi_m T$  value and the value expected for free ions. This procedure guarantees that we use the corrected values for the determination of the CF parameters. Because the interactions between magnetic centers are very weak in this system, this moderate dilution is not expected to have any measurable effect on the static magnetic properties and to produce only a small perturbation on the dynamical behavior compared with a nondiluted crystal.

The CF describes the effect of the electric field due to the surrounding ligands acting on the lanthanoid ion. It splits the electronic ground state multiplet of the free ion, described by its total angular momentum,  $J$ , into  $M_J$  doublets and singlets.

For  $C_5$  symmetry, the CF Hamiltonian can be expressed in terms of the operator equivalents as follows:

$$\hat{H} = \alpha A_2^0 r^2 \hat{O}_2^0 + \beta A_4^0 r^4 \hat{O}_4^0 + \gamma A_6^0 r^6 \hat{O}_6^0 + \gamma A_6^5 r^6 \hat{O}_6^5 \quad (1)$$

where  $\alpha$ ,  $\beta$ , and  $\gamma$  are the Stevens constants for each lanthanoid,<sup>20</sup>  $\hat{O}_k^q$  are the operator equivalents expressed as polynomials of the total angular momentum operators,<sup>21</sup>  $\langle r^k \rangle$  expectation values of the radial factor  $r^k$ , and  $A_k^q$  are numerical parameters that depend on the nature of the ligand shell.

Unlike pseudoaxial systems, where only the  $A_k^q \langle r^k \rangle$  terms with  $q = 0$  ( $A_2^0 \langle r^2 \rangle$ ,  $A_4^0 \langle r^4 \rangle$ ,  $A_6^0 \langle r^6 \rangle$ ) are different from zero, the  $C_5$  symmetry allows a term with  $q = 5$  ( $A_6^5 \langle r^6 \rangle$ ), which mixes magnetic states  $|J, M_J\rangle$  with different  $M_J$ . Therefore,  $M_J$  is no longer a good quantum number. This term appears also in higher symmetries containing axes of order 5, such as the icosahedral symmetry.<sup>22</sup>

As shown in Figure 2, below 50–100 K, the  $\chi_m T$  value of all the samples begins to decrease due to the thermal depopulation

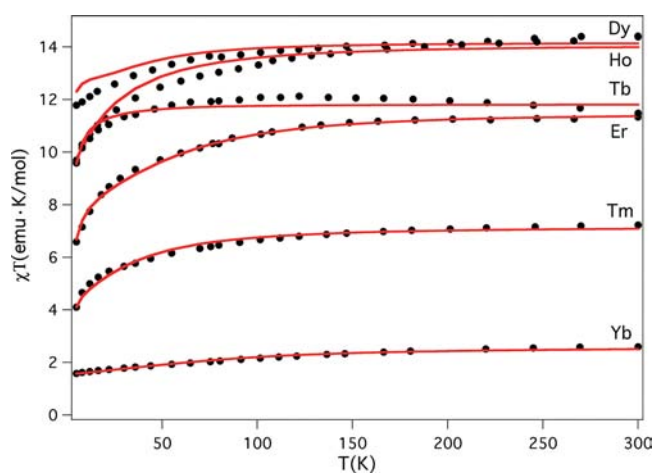


**Figure 2.**  $\chi_m T$  data measured on powdered samples of the  $\text{LnW}_{30}$  series under a magnetic field  $H = 1000 \text{ Oe}$ . The lines are least-squares simultaneous fits of all these curves obtained by the method described above using the CF Hamiltonian (1).

of the excited electronic levels. Thus, in order to determine experimentally the  $A_k^q \langle r^k \rangle$  products, we will make use of the dc magnetic susceptibility data measured as a function of temperature. Ishikawa et al. proposed that the CF parameters of an isomorphic series of lanthanoid complexes could be determined by a simultaneous fit of the all  $\chi_m T$  values under the assumption that the CF parameters from the  $f^8$  to the  $f^3$  system show a linear variation.<sup>23</sup> Under these conditions, the  $A_k^q \langle r^k \rangle$  coefficients can be expressed with eq 2.

$$A_k^q \langle r^k \rangle = a_k^q + b_k^q (n_f - 7) \quad (2)$$

where  $n_f$  goes from 8 to 13 when moving from  $\text{Tb}^{3+}$  to  $\text{Yb}^{3+}$ .

Using this procedure, a good fit of all the magnetic curves has been obtained from a unique set of crystal field parameters (Table 2). The fitting has been made over a set of 40  $\chi_m T$  values per compound. The experimental data were chosen to be approximately equally spaced on a logarithmic temperature scale from 2 K to room temperature in order to give more weight in the fit to the contribution of low energy levels. Figure 2 shows the agreement between the experimental values and the fits.

**Table 2.** CF Parameters Determined for the LnW<sub>30</sub> Series (in cm<sup>-1</sup>)

Ln <sup>3+</sup>	<i>f<sup>n</sup></i>	<i>A</i> <sub>2</sub> <sup>0</sup> < <i>r</i> <sup>2</sup> >	<i>A</i> <sub>4</sub> <sup>0</sup> < <i>r</i> <sup>4</sup> >	<i>A</i> <sub>6</sub> <sup>0</sup> < <i>r</i> <sup>6</sup> >	<i>A</i> <sub>6</sub> <sup>5</sup> < <i>r</i> <sup>6</sup> >
Tb <sup>3+</sup>	8	69.3	34.3	6.7	-1.08 × 10 <sup>3</sup>
Dy <sup>3+</sup>	9	49.7	43.6	11.3	-1.16 × 10 <sup>3</sup>
Ho <sup>3+</sup>	10	30.1	52.9	15.9	-1.24 × 10 <sup>3</sup>
Er <sup>3+</sup>	11	10.5	62.3	20.6	-1.32 × 10 <sup>3</sup>
Tm <sup>3+</sup>	12	-9.1	71.6	25.3	-1.40 × 10 <sup>3</sup>
Yb <sup>3+</sup>	13	-28.68	80.9	29.9	-1.47 × 10 <sup>3</sup>

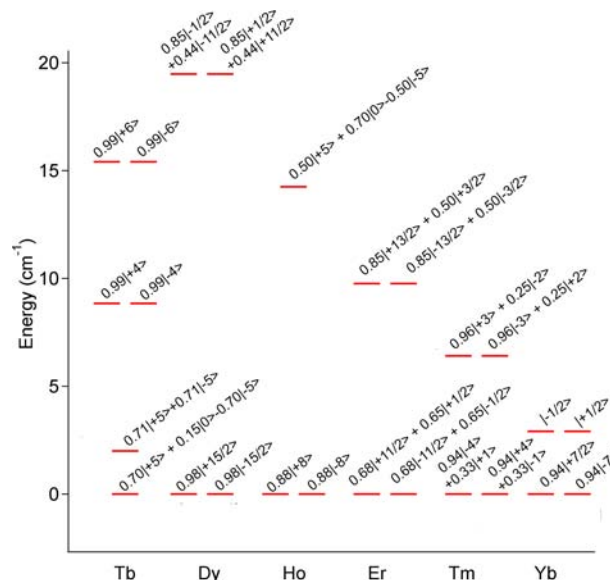
A comparison of these parameters with those found for the [Ln(Pc)<sub>2</sub>]<sup>-</sup> and previous LnPOM families is in order. The most striking contrast appears for the *A*<sub>2</sub><sup>0</sup> parameter, which was positive for all the *D*<sub>4d</sub> phthalocyaninato complexes and negative for all *D*<sub>4d</sub> POM derivatives, while here it depends on the lanthanoid metal. This may be understood when taking into account the position of the ligands in the first coordination sphere (Figure 1): the lanthanoid is slightly between two pentagons formed by oxo atoms from the POM, while the water molecule is on the 5-fold symmetry axis. This means that there is a competition between the closest five oxo ligands from the POM, which are equatorial and contribute negatively to *A*<sub>2</sub><sup>0</sup>, and the apical water molecule, which is axial and contributes to a positive *A*<sub>2</sub><sup>0</sup> value. The five furthest oxygen atoms are very close to the angular node ("magic angle",  $\theta = 54.7^\circ$ ) and their contribution should be smaller than the other two. It is likely that the evolution of this competition could result in a change of sign for the second-order uniaxial parameter. Indeed, a crystallographic and EXAFS study on the lanthanoid series in the Preyssler anion indicates that, as one advances in the series (from Tb<sup>3+</sup> to Er<sup>3+</sup>), the cations tend to move deeper between the pentagons.<sup>24</sup> Because of the angles involved, this can be expected to have a relatively minor effect on the contribution of the closest pentagon and a larger effect on the contribution of the furthest pentagon, resulting in an enhanced negative contribution to *A*<sub>2</sub><sup>0</sup>. Moreover, the metal–water distance tends to grow, diminishing the positive contribution to *A*<sub>2</sub><sup>0</sup>.

The sign of *A*<sub>4</sub><sup>0</sup> is also in contrast with that reported both in phthalocyaninate and in other POM derivatives. Such a difference can also be easily understood. Thus, sandwiched *D*<sub>4d</sub> complexes have all ligands placed around the "magic angle", and hence they contribute negatively to *A*<sub>4</sub><sup>0</sup>. In contrast, in Preyssler complexes, the closest-lying ligands are either axial or (almost) equatorial, which means dominating positive contributions to *A*<sub>4</sub><sup>0</sup>. From this argument, one cannot predict the evolution of *A*<sub>4</sub><sup>0</sup> along the lanthanoid series, since the effects would be competing: decreasing because of the longer distance with both the axial water and the equatorial pentagon vs increasing as the furthest pentagon slips out of the negative lobe.

In a first approximation, the sign and evolution of *A*<sub>6</sub><sup>0</sup> would be similar to those of *A*<sub>2</sub><sup>0</sup>. The fact that our fit produces the opposite result is an indication of the weak dependence of the magnetic data on *A*<sub>6</sub><sup>0</sup>. Hence, these values should only be taken as approximate.

Another difference with the previous *D*<sub>4d</sub> systems is, obviously, the fact that the main extra-diagonal parameter for the Preyssler systems is *A*<sub>6</sub><sup>5</sup> and not *A*<sub>4</sub><sup>4</sup>. Its extremely high absolute value can be understood because, in contrast to what happens in the *D*<sub>4d</sub> case, here the extra-diagonal parameter arises as a first-order effect and not of a small distortion of an ideal structure.

**Electronic Structure of LnW<sub>30</sub>.** The electronic structure within the ground-state *J* multiplet of each lanthanoid is described here. Figure 3 shows the low energy part of the

**Figure 3.** Low-lying levels of the different complexes in the LnW<sub>30</sub> series (Ln = Tb, Dy, Ho, Er, Tm, or Yb).

scheme of the  $2J + 1$  levels obtained by using the set of CF parameters derived from the simultaneous fitting method described above. These schemes are briefly discussed next for each compound in order to predict in which compounds a SMM behavior (i.e., the presence of a superparamagnetic blocking at low *T* with slow relaxation of the magnetization) has to be expected. Before entering into detail, it is important to notice that in contrast to what was observed for *D*<sub>4d</sub> symmetry, for the *C*<sub>5</sub> symmetry the energy levels are, in general, characterized by a pronounced quantum mixture of *M<sub>J</sub>* values (see Table 1, Supporting Information), which will favor the tunneling processes thus making difficult the observation of a SMM behavior. This is a direct consequence of the lowering of the crystal field symmetry (from *D*<sub>4d</sub> to *C*<sub>5</sub>) because it results in the appearance of non-negligible off-diagonal CF parameters (*A*<sub>6</sub><sup>5</sup> in the present case), which allow the mixing of functions with different *M<sub>J</sub>* values.

**TbW<sub>30</sub>.** In this case, the ground state doublet is the *M<sub>J</sub>* = ±5, split by the mixture with *M<sub>J</sub>* = 0. The next sublevel, at 9 cm<sup>-1</sup>, is the *M<sub>J</sub>* = ±4 doublet. Both groups are isolated from all the next levels by a 15 cm<sup>-1</sup> gap. Despite having a high |*M<sub>J</sub>*| ground state, this strong quantum mixture should allow the system to relax and invert its spin, thus preventing the Tb<sup>3+</sup> complex from behaving as a SMM.

**DyW<sub>30</sub>.** The lowest Kramers doublet corresponds to the *M<sub>J</sub>* = ±15/2, the first excited states *M<sub>J</sub>* = ±13/2 and *M<sub>J</sub>* = ±1/2 being placed very near to each other (at 20 cm<sup>-1</sup>). These three doublets are well isolated from the next ones by a gap of about 40 cm<sup>-1</sup>. This may provide a favorable situation for behaving as a SMM.

**HoW<sub>30</sub>.** The ground doublet for this complex is *M<sub>J</sub>* = ±8, and thus, it is favorable for exhibiting SMM behavior. Still, the first excited state, a mixture of *M<sub>J</sub>* = ±5 with *M<sub>J</sub>* = 0, is rather close in energy (only 14 cm<sup>-1</sup> above it). Owing to this small energy

gap, the system is expected to magnetically block only at very low temperatures.

**ErW<sub>30</sub>.** In this complex, the lowest lying doublet is an equally weighted quantum mixture of  $M_J = \pm 11/2$  and  $\pm 1/2$ . The first excited doublet consists of mixtures of  $M_J = \pm 13/2$  and  $\pm 3/2$  and lies at 10 cm<sup>-1</sup> over it. The  $M_J = \pm 15/2$  doublet, responsible for the SMM behavior observed in other POM complexes,<sup>11</sup> is the highest in energy here. This energy scheme should prevent the blocking of its magnetic moment at low temperature.

**TmW<sub>30</sub>.** For this complex, the ground doublet is mainly  $M_J = \pm 4$  with a minor contribution of  $M_J = \mp 1$ . The next doublet is a mixture of  $M_J = \pm 3, \mp 2$ , lying at 7 cm<sup>-1</sup>. In this case, we would expect no direct tunneling, because in a first approximation there is no overlap between the two wave functions containing, respectively,  $\{+4, -1\}$  and  $\{-4, +1\}$ . The experimental lack of SMM properties therefore is in apparent contradiction with the theory and needs a rationalization. A likely explanation is that small distortions to the ideal symmetry can mix the  $M_J = \pm 1$  contribution of the ground doublet, facilitating a rapid relaxation of the magnetization.

**YbW<sub>30</sub>.** The lowest-lying Kramers doublet in this complex is  $M_J = \pm 1/2$ . Two excited doublets have energies close to 3 cm<sup>-1</sup> above the ground state doublet, while the doublet associated with the highest  $M_J$  lies at about 87 cm<sup>-1</sup>. The nearly constant value of  $\chi_m T$  measured below room temperature is probably due to this particular energy level scheme and the ensuing small depopulation of the high CF sublevels. Of course, with the ground state being  $M_J = \pm 1/2$ , no blocking of the magnetization is possible.

**Heat Capacity Measurements.** In view of the above results, the only compounds that are expected to exhibit SMM behavior are the Dy and Ho derivatives. Let us study the molar specific heat,  $c_p$ , of these two compounds to get additional and independent information on the structure of the low-lying magnetic levels. Experimental data for these two compounds are shown in Figures 4 and 5 for different magnetic fields. We next describe the results obtained for each of these two separately.

Above 10 K,  $c_p$  for DyW<sub>30</sub> is dominated by the contribution of lattice vibrations  $c_{\text{latt}}$ . Below 300 K,  $c_{\text{latt}}$  can be fitted reasonably well by the superposition of a Debye function, which accounts for the excitation of acoustic phonon modes with a Debye temperature  $\theta_D = 29(1)$  K, plus two Einstein terms, with characteristic energies  $\varepsilon_{E,1}/k_B = 45$  K and  $\varepsilon_{E,2}/k_B = 108$  K, which account for the contributions of 159 and 321 vibration modes, respectively. At zero field, a magnetic contribution  $c_m$  shows up below 1 K. This contribution arises from the splitting of the magnetic energy levels associated with couplings to other electronic spins, probably of dipolar origin, and the hyperfine interactions with nuclear spins of Dy. This element has two stable isotopes, <sup>161</sup>Dy (natural abundance 18.9%) and <sup>163</sup>Dy (natural abundance 24.9%), with nuclear spin  $I = 5/2$ . A magnetic field further splits each doublet. The splitting of the ground doublet, with  $M_J = \pm 15/2$ , gives rise to the field-dependent Schottky-like anomaly that dominates the specific heat of 2 below 2 K. A second magnetic contribution, visible near 4–9 K, can be associated with the thermal population of the first excited doublet. As is shown in Figure 4, calculations performed with the same CF parameters derived from the magnetic susceptibility account well for the specific heat measured at all fields, therefore giving support to the electronic structure given in Figure 3.

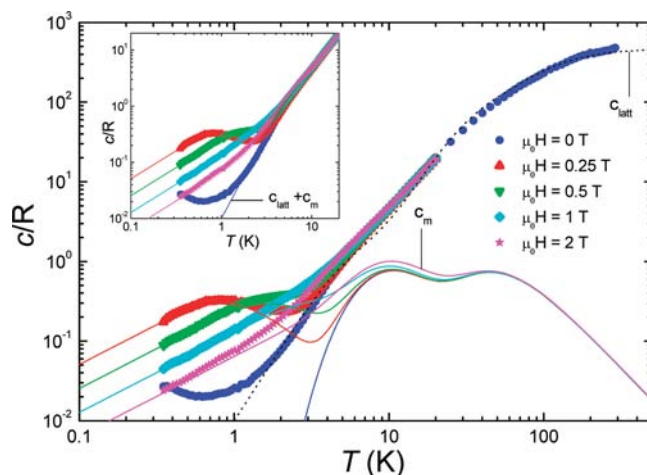


**Figure 4.** Specific heat of a powdered sample of DyW<sub>30</sub> measured at several magnetic fields. The dotted line shows a fit of the lattice contribution  $c_{\text{latt}}$ , whereas the solid lines show the magnetic contribution  $c_m$  calculated with the Hamiltonian (1) using the CF parameters given in Table 2. The inset shows an enlarged view of the low-temperature region. The solid lines give the theoretical  $c_p = c_{\text{latt}} + c_m$ .

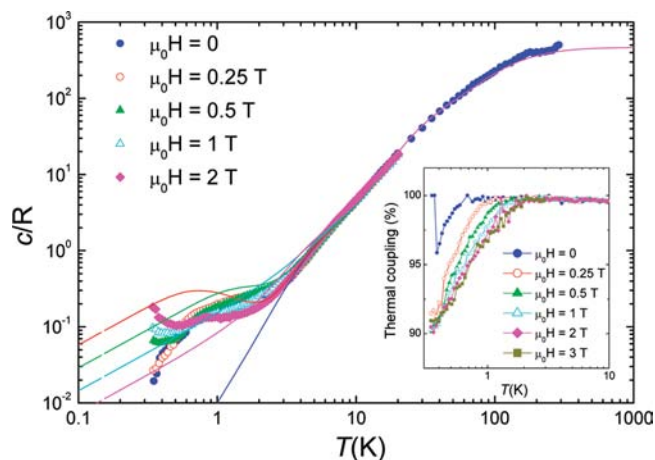


**Figure 5.** Specific heat of a powdered sample of HoW<sub>30</sub> measured at several magnetic fields. The solid lines give the theoretical  $c_p = c_{\text{latt}} + c_m$ . The magnetic  $c_m$  was calculated with the Hamiltonian (1) using the CF parameters given in Table 2. The inset shows the thermal coupling parameters measured at the same field values. Its departure from 100% signals a deviation of the heat capacity from its thermal equilibrium value.

The specific heat of HoW<sub>30</sub> is plotted in Figure 5. Like in the previous sample, lattice vibrations dominate  $c_p$  above 2 K. A good fit of  $c_{\text{latt}}$  is obtained for  $\theta_D = 29(1)$  K,  $\varepsilon_{E,1}/k_B = 45$  K (105 vibration modes), and  $\varepsilon_{E,2}/k_B = 108$  K (375 vibration modes). Measurements performed at  $H = 0$  show the rise of a magnetic contribution  $c_m$  already below 2.5 K. As can be seen by the comparison of Figures 4 and 5, this contribution is larger for the HoW<sub>30</sub> complex than it is for the DyW<sub>30</sub> complex, and furthermore, it shows up at higher temperatures. This is not unexpected, considering the strong hyperfine coupling between electronic and nuclear spins ( $I = 7/2$ ) of <sup>165</sup>Ho (100% natural abundance). This coupling gives rise to a series of electro-nuclear energy levels defined by the electronic  $M_J$  and nuclear  $M_I$  spin projections along  $z$ , with approximate energies  $E_{\text{hf}}(M_J M_I) = M_J A_{\text{hf}} M_I / k_B$  where  $A_{\text{hf}}/k_B = 0.04$  K is the

hyperfine coupling constant. The overall hyperfine splitting in the ground electronic doublet  $M_J = \pm 8$  is  $\Delta E_{\text{hf}}/k_B \approx 7M_J A_{\text{hf}}/k_B \approx 2.3$  K. By contrast, only 42% Dy atoms carry a nuclear spin, and the hyperfine coupling  $A_{\text{hf}}$  is nearly 8 times weaker than that of Ho.

Data measured under nonzero magnetic fields also show a magnetic contribution, which appears to gradually shift toward higher temperatures, as in  $\text{DyW}_{30}$ . However, the experimental  $c_m$  remains smaller than the expected electronic contribution (i.e., arising only from the electronic magnetic moments), which is shown by the solid lines in Figure 5. This effect suggests that the populations of electronic and nuclear spin levels are not able to fully attain their thermal equilibrium values within the experimental time scales. The time scale, on the order of 1.5 s at 1 K, is determined, in the present experiments, by the duration of the heat power pulses applied to the calorimeter. If  $c_m$  depends on time, the temperature changes that follow each pulse deviate from a pure exponential decay. This is observed here, indeed, as witnessed by the decrease of the effective thermal coupling, shown in the inset of Figure 5, with decreasing temperature. This parameter gives a measure of how closely the temperature decay follows an exponential decay, thus also of the presence of nonequilibrium effects in  $c_p$ . Therefore, these data show that the re-equilibration of electronuclear magnetic levels becomes relatively slow below 2 K, the more so as the magnetic field increases. These phenomena have been observed in polynuclear magnetic clusters, such as  $\text{Mn}_{12}$ ,  $\text{Fe}_8$ ,  $\text{Mn}_4$ , and others, where they are associated with the slow magnetic relaxation characteristic of the SMM behavior.<sup>25–27</sup> These aspects are considered in more detail in the following section.

**Inelastic Neutron Scattering Experiments.** INS was pursued in the instrument IN4 of the ILL for the compounds  $\text{K}_{12}\text{DyP}_5\text{W}_{30}\text{O}_{110}$  and  $\text{K}_{12}\text{HoP}_5\text{W}_{30}\text{O}_{110}$ , because it is a technique that generally produces high-quality spectroscopic information on these excited magnetic levels. The measurements were done at wavelengths  $\lambda = 1.1, 2.2,$  and  $3.6$  Å, which correspond to energy windows of 5–60, 2–15, and 1–5 meV. Unfortunately, we found that the spectra are dominated by very intense phonon transitions that obscure any magnetic signal of the lanthanoid. Hence, INS has not provided in this case any information on this energy gap. The INS spectra are shown in Figures S1–3, Supporting Information.

**Dynamic Susceptibility and Magnetization Hysteresis Measurements.** Alternating current susceptibility measurements have been performed for the six members of the  $\text{LnW}_{30}$  series above 2 K. As expected, in this temperature region only the susceptibilities of samples with  $\text{Dy}^{3+}$  and  $\text{Ho}^{3+}$  depend on frequency. The dependences of  $\chi'$  and  $\chi''$  are compatible with Cole–Cole functions<sup>28</sup> with  $\alpha \leq 0.2$ , as expected for a SMM relaxing its magnetic moment via a thermally activated mechanism. Yet, even in these two samples, a complete blocking of the susceptibility is not observed. In order to better understand the relaxation processes that govern the spin dynamics in these samples, ac susceptibility and magnetization hysteresis experiments have been extended to the region of very low temperatures. For the  $\text{DyW}_{30}$ , the in-phase  $\chi'$  and out-of-phase  $\chi''$  components of the ac susceptibility are shown in Figure 6. Remarkably enough, the two curves increase with decreasing temperature down to 80 mK; that is, no complete superparamagnetic blocking occurs. This behavior indicates that the magnetic relaxation rate,  $\tau^{-1}$ , depends very weakly on temperature.

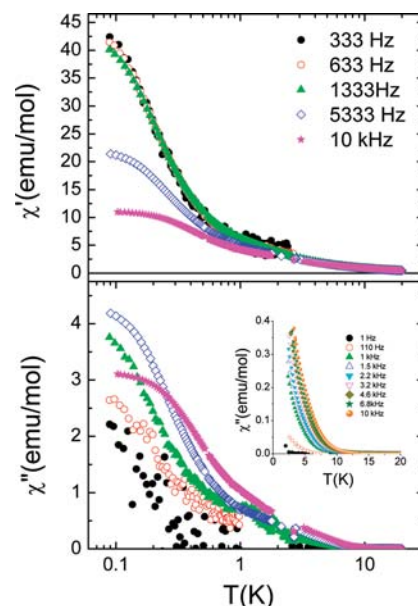


**Figure 6.** Alternating current susceptibility of a powdered sample of  $\text{DyW}_{30}$  vs temperature (in logarithmic scale): (top) in-phase component; (bottom) out-of-phase component. The inset shows an enlarged view of  $\chi''$  measured above 2 K.

The relaxation rate has been estimated as  $\tau = \chi''/(\omega\chi')$ . Strictly speaking, this relation holds only in the limit  $\omega \rightarrow 0$ . However, it provides a reasonably good approximation for frequencies that fulfill the condition  $\omega\tau \ll 1$ . Results obtained for  $\omega/(2\pi) = 13.3$  kHz are shown in Figure 7. The magnetic

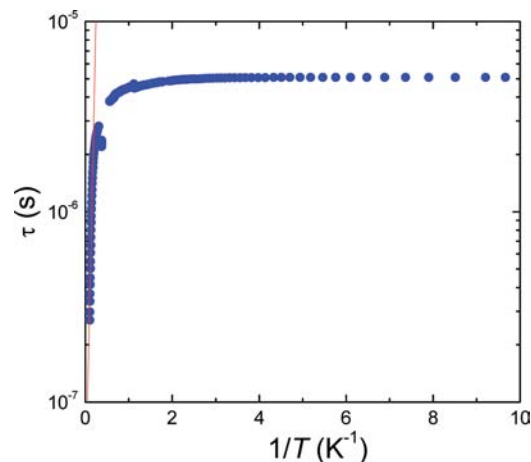


**Figure 7.** Relaxation-time plot used to fit an Arrhenius law for  $\text{DyW}_{30}$  at zero magnetic field.

relaxation is thermally activated above 2 K. Between 5 and 10 K, the Arrhenius fit of  $\tau$  vs  $1/T$  gives an activation energy  $U/k_B = 24$  K. If we consider the electronic energy level spectrum of this complex (see Figure 2), these results suggest that, in this temperature region, magnetic relaxation takes place via thermal excitations to the first excited doublet. Between approximately 5 and 2 K, the relaxation time gradually flattens, finally saturating, below 2 K, to a very short value  $\tau \approx 5$  μs, thus showing that relaxation becomes then dominated by pure quantum tunneling processes. The crossover to a new relaxation mechanism also leaves its mark on the distribution of relaxation times. Below 2 K, the parameter  $\alpha$  of the Cole–

Cole functions increases to about 0.3–0.35. This increase can be assigned to the strong sensitivity of pure quantum tunneling events to the magnitude of the local magnetic bias acting on each spin.<sup>29</sup> At zero applied field, the bias is mainly associated with intercluster dipolar magnetic interactions. Because the molecular spins are oriented at random (the sample is paramagnetic), the dipolar bias changes from one lattice point to another, thus giving rise to a distribution of tunneling times.

The data of Figure 8 show that the relaxation time increases by at least 1 order of magnitude when low-intensity magnetic

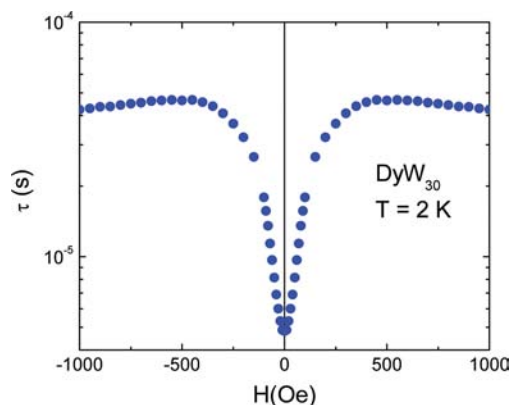


**Figure 8.** Magnetic relaxation time of a powdered DyW<sub>30</sub> sample versus magnetic field.

fields are applied. This leads to observable magnetization hysteresis below 2 K, as is shown in Figure 9. These results confirm the SMM behavior and that spin–lattice relaxation occurs via pure quantum tunneling, as has recently been observed for ErW<sub>10</sub>.<sup>11</sup>

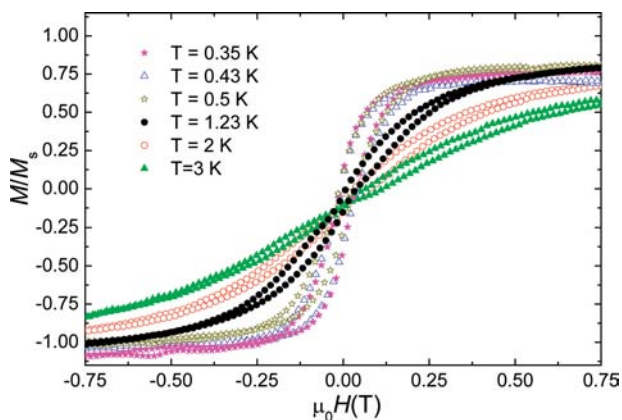


**Figure 9.** Hysteresis curves measured on powdered DyW<sub>30</sub> at very low temperatures. The magnetic field sweeping rate was 2 T/min.

For HoW<sub>30</sub>, the in-phase and out-of-phase susceptibility components are shown in Figure 10. They show evidence for a superparamagnetic blocking but only at very low temperatures. The relaxation time, shown in the inset of Figure 10, was determined from the maxima of  $\chi''$  vs  $T$  curves measured at different frequencies. The activation energy estimated from the Arrhenius plot is  $U/k_B \approx 0.8$  K, much smaller than the energy separation between the first excited level and the ground level doublet  $M_J = \pm 8$ , which amounts to approximately  $14 \text{ cm}^{-1}$ .

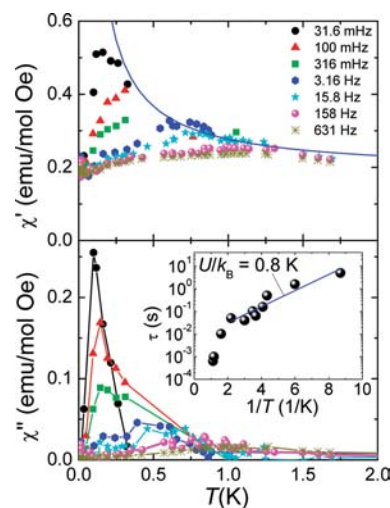


**Figure 10.** Alternating current susceptibility of a HoW<sub>30</sub> single crystal having the magnetic anisotropy axis ( $C_5$  symmetry axis of the lanthanoid coordination shell, cf Figure 1) oriented at approximately  $86.5^\circ$  with respect to the excitation magnetic field: (top) in-phase component; the solid line is the equilibrium susceptibility  $\chi_m$  calculated with eq 2 and the CF parameters given in Table 2; (bottom) out-of-phase component. The inset shows the Arrhenius plot of the relaxation time  $\tau$ .

This shows that the low- $T$  relaxation involves only transitions within the electronic ground state doublet.

The activated behavior, which contrasts with the nearly temperature-independent relaxation observed for DyW<sub>30</sub>, can be associated with the strong hyperfine splitting present in Ho. Quantum tunneling takes place preferentially between states with the same nuclear spin projection  $M_I$ . Since the ground states of the electronuclear spin system have opposite  $M_I$ , the hyperfine interaction is to some extent equivalent to a bias field, blocking pure quantum tunneling. This effect has been observed in Ho-based phthalocyanines.<sup>30</sup> There, it was shown that quantum tunneling transitions between  $M_I$  and  $-M_I$  states can be induced by the application of an external magnetic field, which generates level crossings between states of equal  $M_I$ . Our results add complementary information to this picture. They show that, at zero field, magnetic relaxation takes place by thermally activated transitions to excited nuclear spin states. Within this picture, the SMM behavior is dictated by hyperfine interactions rather than by the strength of the magnetic anisotropy. The prefactor  $\tau_0 = 6 \times 10^{-3}$  s must then be associated with the lifetime of such excited nuclear spin states. The existence of such long-lived states is fully compatible with the weak coupling of nuclear spins to the lattice.

The SMM behavior is confirmed by the observation of magnetization hysteresis below 2 K (Figure 11). This temperature is much higher than the blocking temperatures determined from ac susceptibility experiments, which are all well below 1 K even for relatively high frequencies. The enormous differences between the spin dynamics measured by these two experimental techniques suggest that, similarly to what happens in the case of DyW<sub>30</sub>, the magnetic relaxation time of HoW<sub>30</sub> increases very strongly with  $H$ . The extreme sensitivity of  $\tau$  to external magnetic fields seems to be a characteristic trait of mononuclear SMMs.<sup>12,31</sup>

Before closing this section, we shall consider the origin of the nonequilibrium phenomena observed in the specific heat of HoW<sub>30</sub>. At zero field,  $c_m$  deviates from equilibrium below

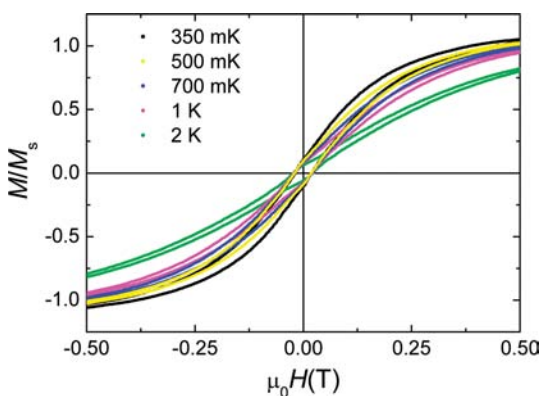


**Figure 11.** Magnetization hysteresis loops of  $\text{HoW}_{30}$  measured at different temperatures. The magnetic field sweeping rate was 0.54 T/min.

approximately 0.6 K, for experimental time scales on the order of 1 s. At the same temperature, the spin–lattice relaxation time obtained from the ac susceptibility is much shorter, on the order of 0.01 s. Since the two experiments are performed at zero field, the difference cannot be ascribed to the dependence of  $\tau$  on  $H$ . Rather, it shows that both quantities are sensitive to different spin–lattice relaxation times: while the ac susceptibility gives mainly information about the relaxation of electronic spins, the low- $T$  specific heat data depend on the re-equilibration of all electronuclear spin levels. Therefore, although both processes are intimately linked in Ho, our data suggest that the nuclear spin–lattice relaxation is much slower than the electronic spin–lattice relaxation.

## CONCLUDING REMARKS

In this work, we have shown that POM-based mononuclear lanthanoid complexes with 5-fold symmetry can provide new examples of single-ion magnets that exhibit magnetic hysteresis at low temperatures in the case of Dy and Ho. This very unusual crystal field symmetry gives rise to remarkably large off-diagonal anisotropy parameters  $A_6^5$ , which mix magnetic states with different  $M_J$  values. The spin dynamics, especially at low temperatures, is then dominated by fast tunneling processes and is strongly affected by hyperfine interactions and external magnetic fields. The fast spin–lattice relaxation associated with fast quantum tunneling seems to be detrimental for the use of these molecular single-ion magnets as magnetic memories. However, it can provide very attractive candidates for the application as solid-state spin qubits. In fact, most of these molecules possess a well-defined ground state doublet, which provides a good definition for the qubit state basis. The high tunneling rates should enable the coherent manipulation of these two states, for example, by using external electromagnetic radiation. In this respect, the existence, for some lanthanoids, of a manifold of electronuclear states can provide additional resources for the implementation of multiple qubit states within the same molecule.<sup>32</sup> This aspect is particularly relevant when dealing with POM molecules, because in this class of coordination complexes the main sources of quantum decoherence (hyperfine couplings and dipolar spin–spin interactions) can be minimized by preparing nuclear-spin free compounds and by diluting the magnetic centers while conserving the crystallinity. The ability of POMs to accommodate the lanthanoids in very different symmetries ( $D_{4d}$  vs  $C_5$ ) offers also the possibility of tuning the magnetic

anisotropy in these nanomagnets, while keeping them magnetically isolated (the magnetic ordering in these materials only occurs at very low temperatures; typically below 0.01 K). All these results allow us to emphasize that (i) mononuclear single-ion magnets offer very attractive possibilities to design new molecular nanomagnets with a control over their magnetic properties that is almost impossible to achieve with polynuclear clusters and dominant quantum effects and (ii) POM chemistry provides ideal examples of SIMs based on lanthanoids, which have shown to be useful as spin qubits<sup>33</sup> or, very recently, as magnetic coolers for ultralow temperatures.<sup>34</sup>

## ASSOCIATED CONTENT

### Supporting Information

Energies and modulus of the contribution of each  $M_J$  to the wavefunctions of the ground state multiplets and inelastic neutron scattering spectra. This information is available free of charge via the Internet at <http://pubs.acs.org>.

## AUTHOR INFORMATION

### Corresponding Author

eugenio.coronado@uv.es; fluis@unizar.es

### Notes

The authors declare no competing financial interest.

## ACKNOWLEDGMENTS

The present work has been funded through the EU (Project ELFOS and ERC Advanced Grant SPINMOL), the Spanish MINECO (Grants MAT2011-61584, MAT2009-13977-C03, MAT2007-61584, CTQ2008-06720 and the CONSOLIDER project on Molecular Nanoscience, CSD-2007-00010), the Generalidad Valenciana (Prometeo and ISIC Programmes of Excellence), and the Gobierno de Aragón (Project MOLCHIP). The authors thank Dr. Hannu Mutka and the Institut Laue-Langevin for the INS measurements and the later discussion about the results. S.C.-S. also thanks the Spanish MECED for a FPU predoctoral grant.

## REFERENCES

- (a) Clemente-Juan, J. M.; Coronado, E. *Coord. Chem. Rev.* **1999**, *193–195*, 361–394. (b) Kortz, U.; Müller, A.; van Slageren, J.; Schnack, J.; Dalal, N. S.; Dressel, M. *Coord. Chem. Rev.* **2009**, *253*, 2315–2327.
- (a) Suaud, N.; Gaita-Ariño, A.; Clemente-Juan, J. M.; Sánchez-Marín, J.; Coronado, E. *J. Am. Chem. Soc.* **2002**, *124*, 15134–15140. (b) Borrás-Almenar, J. J.; Clemente-Juan, J. M.; Coronado, E.; Tsukerblat, B. *Chem. Phys.* **1995**, *195*, 1–15.
- Calzado, C. J.; Clemente-Juan, J. M.; Coronado, E.; Gaita-Ariño, A.; Suaud, N. *Inorg. Chem.* **2008**, *47*, 5889–5901.
- (a) Coronado, E.; Gómez-García, C. J. *Comments Inorg. Chem.* **1995**, *17*, 255–281. (b) Bassil, B. S.; Kortz, U. *Z. Anorg. Allg. Chem.* **2010**, *636*, 2222.
- Müller, A.; Peters, F.; Pope, M. T.; Gatteschi, D. *Chem. Rev.* **1998**, *98*, 239–271.
- Kögerler, P.; Tsukerblat, B.; Müller, A. *Dalton Trans.* **2010**, *39*, 21–36.
- Palii, A.; Tsukerblat, B.; Klokishner, S.; Dunbar, K.; Clemente-Juan, J. M.; Coronado, E. *Chem. Soc. Rev.* **2011**, *40*, 3130–3156.
- Lehmann, J.; Gaita-Ariño, A.; Coronado, E.; Loss, D. *Nat. Nanotechnol.* **2007**, *2*, 312–317.
- (a) Lehmann, J.; Gaita-Ariño, A.; Coronado, E.; Loss, D. *J. Mater. Chem.* **2009**, *19*, 1672–1677. (b) Clemente-Juan, J. M.; Coronado, E.; Gaita-Ariño, A. *Chem. Soc. Rev.* **2012**, DOI: 10.1039/c2cs35205b.
- Bertaina, S.; Gambarelli, S.; Mitra, T.; Tsukerblat, B.; Müller, A.; Barbara, B. *Nature* **2008**, *453*, 203–206.

- (11) (a) Aldamen, M. A.; Clemente-Juan, J.; Coronado, E.; Martí-Gastaldo, C.; Gaita-Ariño, A. *J. Am. Chem. Soc.* **2008**, *130*, 8874–8875. (b) Aldamen, M. A.; Cardona-Serra, S.; Clemente-Juan, J. M.; Coronado, E.; Gaita-Ariño, A.; Martí-Gastaldo, C.; Luis, F.; Montero, O. *Inorg. Chem.* **2009**, *48*, 3467–3479.
- (12) Luis, F.; Martínez-Pérez, M.; Montero, O.; Coronado, E.; Cardona-Serra, S.; Martí-Gastaldo, C.; Clemente-Juan, J. M.; Sesé, J.; Drung, D.; Schurig, T. *Phys. Rev. B* **2010**, *82*, No. 060403.
- (13) Ishikawa, N.; Sugita, M.; Ishikawa, T.; Koshihara, S. Y.; Kaizu, Y. *J. Am. Chem. Soc.* **2003**, *125*, 8694–8695.
- (14) Ishikawa, N.; Sugita, M.; Ishikawa, T.; Koshihara, S.; Kaizu, Y. *J. Phys. Chem. B* **2004**, *108*, 11265–11271.
- (15) (a) Bertaina, S.; Gambarelli, S.; Tkachuk, A.; Kurkin, I. N.; Malkin, B.; Stepanov, A.; Barbara, B. *Nature Nano.* **2007**, *2*, 39–42. (b) Coronado, E.; Giménez-Saiz, C.; Recuenco, A.; Tarazón, A.; Romero, F. M.; Camón, A.; Luis, F. *Inorg. Chem.* **2011**, *50*, 7370–7372. (c) Jiang, S.; Wang, B.; Sun, H.; Wang, Z.; Gao, S. *J. Am. Chem. Soc.* **2011**, *133*, 4730–4733.
- (16) Creaser, I.; Heckel, M. C.; Neitz, R. J.; Pope, M. T. *Inorg. Chem.* **1993**, *32*, 1573–1578.
- (17) Martínez-Pérez, M. J.; Sesé, J.; Luis, F.; Drung, D.; Schurig, T. *Rev. Sci. Instrum.* **2010**, *81*, No. 0161198.
- (18) Kim, K.-C.; Pope, M. T.; Gama, G. J.; Dickman, M. H. *J. Am. Chem. Soc.* **1999**, *121*, 11164–11170.
- (19) Creaser, I.; Heckel, M.; Neitz, R.; Pope, M. *Inorg. Chem.* **1993**, *32*, 1573–1578.
- (20) Stevens, K. W. H. *Proc. Phys. Soc. A* **1952**, *65*, 209–215.
- (21) (a) Orbach, R. *Proc. Phys. Soc. A* **1961**, *264*, 458–484. (b) Rudowicz, C. *J. Phys. C: Solid State Phys.* **1985**, *18*, 1415–1430.
- (22) Walter, U. *Phys. Rev. B* **1987**, *36*, 2504–2512.
- (23) Ishikawa, N.; Sugita, M.; Okubo, T.; Takana, N.; Iino, T.; Kaizu, Y. *Inorg. Chem.* **2003**, *42*, 2440–2446.
- (24) Chiang, M.-H.; Antonio, M. R.; Williams, C.; Soderholm, L. *Dalton Trans.* **2004**, *5*, 801–806.
- (25) Sessoli, R.; Tsai, H.-L.; Schake, A.; Wang, S.; Vincent, J.; Folting, K.; Gatteschi, D.; Christou, G.; Hendrickson, D. N. *J. Am. Chem. Soc.* **1993**, *115*, 1804–1816.
- (26) Delfs, C.; Gatteschi, D.; Pardi, L.; Sessoli, R.; Wieghardt, K.; Hanke, D. *Inorg. Chem.* **1993**, *32*, 3099–3103.
- (27) Aliaga-Alcalde, N.; Edwards, R.; Hill, S.; Wernsdorfer, W.; Folting, K.; Christou, G. *J. Am. Chem. Soc.* **2004**, *126*, 12503–12516.
- (28) Cole, K. H.; Cole, R. H. *J. Chem. Phys.* **1941**, *9*, 341–352.
- (29) Wernsdorfer, W.; Ohm, T.; Sangregorio, C.; Sessoli, R.; Mailly, D.; Paulsen, C. *Phys. Rev. Lett.* **1999**, *82*, 3903–3906.
- (30) Ishikawa, N.; Sugita, M.; Wernsdorfer, W. *J. Am. Chem. Soc.* **2005**, *127*, 3650–3651.
- (31) Car, P. E.; Perfetti, M.; Mannini, M.; Favre, A.; Caneschi, A.; Sessoli, R. *Chem. Commun.* **2011**, *47*, 3751–3753.
- (32) Bertaina, S.; Gambarelli, S.; Tkachuk, A.; Kurkin, I. N.; Malkin, B.; Stepanov, A.; Barbara, B. *Nat. Nanotechnol.* **2007**, *2*, 39–42.
- (33) Martínez-Pérez, M. J.; Cardona-Serra, S.; Schlegel, C.; Moro, F.; Alonso, P. J.; Prima-García, H.; Clemente-Juan, J. M.; Evangelisti, M.; Gaita-Ariño, A.; Sesé, J.; van Slageren, J.; Coronado, E.; Luis, F. *Phys. Rev. Lett.* **2012**, *108*, No. 247213.
- (34) Martínez-Pérez, M. J.; Montero, O.; Evangelisti, M.; Luis, F.; Sesé, J.; Cardona-Serra, S.; Coronado, E. *Adv. Mater.* **2012**, *24*, 4301–4305.